Structural dissipative solitons in passive mode-locked fiber lasers

Andrey Komarov* and François Sanchez
Laboratoire POMA, FRE CNRS 2988, Université d'Angers, 2 Bd Lavoisier, 49000 Angers, France
(Received 21 February 2008; published 3 June 2008)

On the basis of numerical simulation of fiber laser passive mode locking with anomalous dispersion we have found the dissipative solitons with powerful pedestals having oscillating structure. The pedestal structure causes a complex structural spectrum. These solitons can be multistable: with the same laser parameters the pedestals can have different structures. For some nonlinear-dispersion parameters there exist solitons with asymmetric structural pedestals moving relatively solitons with symmetric ones.

DOI: 10.1103/PhysRevE.77.066201 PACS number(s): 89.75.Kd, 42.60.Fc, 42.65.Sf, 42.65.Tg

I. INTRODUCTION

Stable self-localized waves called solitons are one of the most fascinating nonlinear phenomena. Indeed, they arise widely in diverse fields of physics [1,2]. For instance, solitons appear in problems of hydrodynamics, plasma physics, superfluidity, or nonlinear optics including laser passive mode locking. Among the various nonlinear systems, the passive mode-locked fiber lasers holds a peculiar place. Thanks to the possibility to change nonlinear-dispersion parameters in a very large range, this type of laser systems provides high potentialities for investigation of diverse soliton properties.

In many cases, the analysis of nonlinear dynamics of solitons, including dissipative solitons in passive mode-locked fiber lasers, is based on various versions of complex Ginzburg-Landau equation (CGLE) [3]. The cubic CGLE describes the passive mode locking with single soliton inside a laser cavity [4]. The spectral and spatial intensity distributions of such soliton are symmetric and have bell-shaped profiles. The inclusion of higher-order nonlinearities results in multisoliton formation in passive mode locking [5,6]. In the paper [5] the multisoliton operation was obtained in the frame of the cubic-quintic CGLE. In the paper [6] it was used the more complicated version of the CGLE which describes adequately the nonlinear losses forming ultrashort pulses due to the nonlinear polarization rotation technique. Theses solitons in multiple pulse regimes have the same spectral and spatial parameters that is caused by the effect of quantization of intracavity radiation into individual identical ultrashort pulses. The multisoliton operation was experimentally observed in fiber and other lasers. In the case of pulse attraction, the structures of bound solitons are formed [7,8]. As a rule, these structures have symmetric spectral and spatial-intensity profiles. However, with certain laser parameters, they can be asymmetric [9]. Such multisoliton structures with left and right asymmetries move relative to each other, to symmetric structures, and to the isolated pulses.

In this paper we have found that the individual isolated solitons in fiber lasers can also have an intrinsic structure. It is related with the structure of soliton pedestal. The pedestal structure can depend on initial conditions. This dependence can be a multivalued function, that is, such isolated soliton is multistable. The powerful pedestal with structural properties is realized in the case of anomalous net frequency dispersion of intracavity fiber medium. In the case of an asymmetric pedestal, the structural solitons with left and right asymmetry move relatively each to other, relatively to the symmetric solitons and to the symmetric soliton structures. Our study is based on numerical simulation with using the CGLE taking into account the real characteristics of nonlinear losses in passive mode-locked fiber lasers with the nonlinear polarization rotation technique.

In Sec. II we present the model of a passive mode-locked fiber laser with nonlinear polarization rotation technique. Here we also present the corresponding equations describing the soliton dynamics and results of numerical simulation. The effects of period doubling for intracavity solitons are typical for passive mode-locked laser models with lumped nonlinear losses [10]. These effects mask the investigated phenomena. To preclude this masking, in Sec. III we study the discussed phenomena in the frame of distributed models including the model described by cubic-quintic CGLE. Section IV is devoted to the discussion of the obtained results.

II. FIBER LASER WITH LUMPED NONLINEAR LOSSES

A. Physical model and master equations

The passive mode locking in investigated fiber laser is realized through nonlinear polarization rotation for an intracavity light wave. We use typical parameters for an erbium-doped fiber laser. Figure 1 shows the studied laser system which is described in detail in Ref. [6]. This system involves

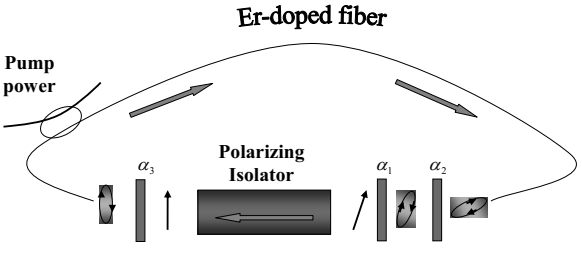

FIG. 1. Schematic representation of the investigated laser.

*Permanent address: Institute of Automation and Electrometry, Russian Academy of Sciences, Acad. Koptyug Pr. 1, 630090 Novosibirsk, Russia.

all necessary elements for the control of nonlinear losses. After the polarizing isolator the electric field has a linear polarization. Such state of polarization does not experience polarization rotation in the fiber because the rotation angle is proportional to the area of the polarization ellipse. Consequently, it is necessary to place a quarter wave plate 3 (α_3 represents the orientation angle of one eigenaxis of the plate with respect to the laboratory frame). The rotation of the polarization ellipse resulting from the optical Kerr nonlinearity is proportional to the light intensity, the area of the polarization ellipse and the fiber length. At the output of the fiber, the direction of the elliptical polarization of the central part of the pulse can be rotated towards the passing axis of the polarizer by the half wave plate 2 (the orientation angle is α_2). Then this elliptical polarization can be transformed into a linear one by the quarter wave plate 1 (the orientation angle is α_1). In this situation the losses for the central part of the pulse are minimum while the wings undergo strong losses.

The resulting model assumes localized effect for the nonlinear losses due to the Kerr nonlinearity combined with the phase plates and the polarizer, while gain and group-velocity dispersion are distributed along the fiber. In dimensionless form, the final set of equations for the electric field amplitude is

$$\frac{\partial E}{\partial \zeta} = (D_r + iD_i)\frac{\partial^2 E}{\partial \tau^2} + (G + iq|E|^2)E, \tag{1}$$

$$E_{n+1}(\tau) = -\eta[\cos(pI_n + \alpha_0)\cos(\alpha_1 - \alpha_3) + i\sin(pI_n + \alpha_0)\sin(\alpha_1 + \alpha_3)]E_n(\tau), \tag{2}$$

where $E(\zeta,\tau)$ is the electric field amplitude, τ is a time coordinate expressed in units $\delta t = \sqrt{|\beta_2|L/2}$ (here β_2 is the second-order group-velocity dispersion for fiber and L is the fiber length), ζ is the normalized propagation distance (ζ varies from 0 to 1 in a roundtrip), D_r and D_i are the frequency dispersions for a gain-loss and for a refractive index, respectively, q is the Kerr nonlinearity.

The term G in the second parenthesis in Eq. (1) describes the saturable amplification determined by the total energy of the intracavity radiation

$$G = \frac{a}{1 + b\int |E|^2 d\tau}, \tag{3}$$

where the integration is carried out on the whole roundtrip period, a is the pumping parameter, b is the saturation one. The second term in these parentheses is connected with Kerr nonlinearity of the fiber. Equation (2) determines the relation between the time distributions of the field before and after nth pass of radiation through the polarizer (η is the transmission coefficient of the intracavity polarizer). The values α_1, α_3, α_2 are orientation angles of the quarter wave plates 1, 3 and of the half wave plate 2, respectively. Parameters α_0, I, p are determined by relations $\alpha_0 = 2\alpha_2 - \alpha_1 - \alpha_3$, $I = |E|^2$, $p = \sin(2\alpha_3)/3$. The amplitude $E(\tau)$ is subject to periodic boundary conditions with period equal to one roundtrip.

The description of the gain G by Eq. (3) is correct for the steady-state regimes and for transient process for which the gain is sufficiently closed to the equilibrium value which is determined by the equilibrium between the pump and the light induced depletion of the gain. It is precisely these lasing operations that are studied in this paper. It is evident that in the general case (for example, in the case of spike regimes), it is necessary to take into account the finiteness of the gain medium relaxation time [11].

For numerical simulation we use the standard split-step Fourier method connected with splitting the nonlinear-dispersion task into nonlinear and dispersion parts. After each total pass of resonator the field $E(\tau)$ is transformed with correspondence with Eq. (2) that is due to the nonlinear losses in the polarizer. Equations (1)–(3) allow us to determine the evolution of field in the laser cavity.

B. Results of numerical simulation

Numerical simulation has been performed for typical parameters of Er-doped fiber laser with the anomalous net dispersion of group velocity. As one can see from Figs. 2 and 3 in the case of anomalous dispersion the dissipative soliton can have the powerful pedestal with oscillating structure in the temporal distribution of the intensity. This structure manifests itself as the periodic spectral structure superimposing on a bell-shaped spectral profile of a standard ultrashort pulse. The spectral and temporal structures of the soliton are critical for changes of laser parameters. In the case of Figs. 2 and 3 a small change in the dispersion D_i induces drastic changes in the spectrum and in the pedestal of the ultrashort pulse. For the used laser parameters, the top part of the soliton is mainly formed by the combined action of focusing nonlinearity ($q>0$) and anomalous dispersion ($D_i>0$) of refractive index. The peak intensity is determined by the orientation angles of the intracavity phase plates. The formation of the pedestal is essentially determined by the nonlinear losses.

With the same laser parameters the structures of the soliton pedestal can be different. This fact is demonstrated by Fig. 4. The spectral and temporal distributions in Figs. 4(a) and 4(b) and in Figs. 4(c) and 4(d) correspond to two solitons with different pedestals which are realized with the same laser parameters. The realization of one or the other soliton depends on initial conditions. The transition from one type of soliton to the other with changing dispersion D_i is determined by an hysteresis phenomena. Figure 5(a) shows this hysteresis through the dependence of the soliton energy J on the dispersion D_i. With decreasing D_i from 1 until 0.92 the soliton energy increases that shows the upper branch of the dependence $J=J(D_i)$ [straight line in Fig. 5(a)]. For this branch the type of soliton corresponds to the one shown in Figs. 4(c) and 4(d). In point $D_i=0.92$ the soliton structure switches towards the structure shown in Figs. 4(a) and 4(b). In transient process, during switching, we observed the period-doubling operation with alternative realization of these two type of solitons after each pass of radiation through the laser cavity. With increasing dispersion D_i from 0.90 until 0.94 the stationary soliton with the structure shown

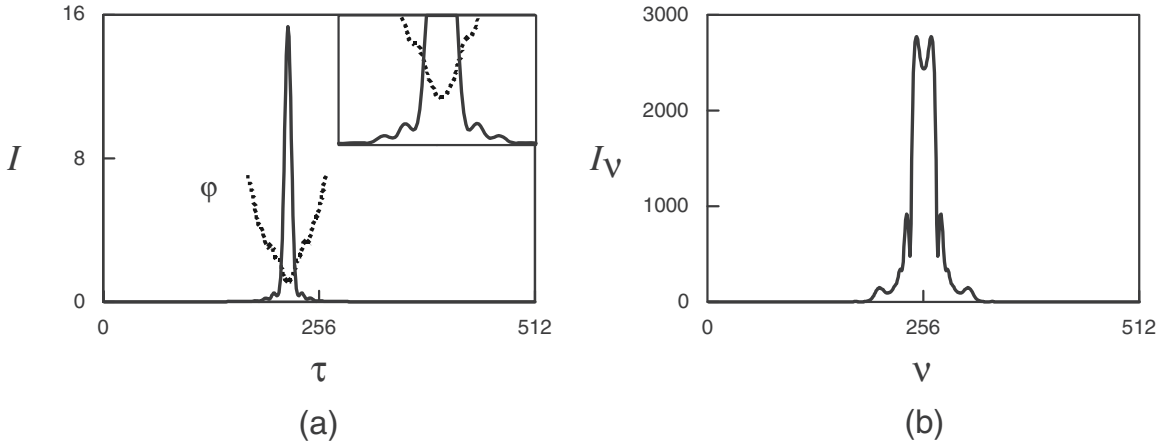

FIG. 2. Temporal (a) and spectral (b) distributions of radiation for dissipative soliton in the fiber laser with anomalous net frequency dispersion of intracavity medium. The change of phase φ along the soliton is shown by the dash curve in (a). The upper right inset in (a) shows the multiplied soliton pedestal. In all figures we use arbitrary units. $a=1.05$, $q=1$, $D_i=1.1$, $\alpha_0=0.1$, $\alpha_1=-1.74$, $\alpha_3=0.1$. D_r is determined by the amplification medium: $D_r=D_{r0}G$, $D_{r0}=0.26$.

in Figs. 4(a) and 4(b) is realized. After the point $D_i=0.94$ the soliton energy changes chaotically from one pass of radiation through the laser resonator to another. In the point $D_i=0.97$ the regime becomes stationary with the soliton structure shown in Figs. 4(c) and 4(d). Figure 5(b) demonstrates the typical dependence $J=J(D_i)$ due to effects of period doubling [12,13]. One can see the regions of D_i where the soliton structure is repeated after two roundtrip periods, after four ones, and is changed chaotically at each pass of radiation through the cavity. Here the dependence of energy J on the number of passes n demonstrates undamped periodical and chaotic oscillations. As pointed out above, in transient process, during switching from the upper branch into the lower in the dependence $J=J(D_i)$ at the point $D_i=0.92$ [see Fig. 5(a)], we observed the similar oscillations with double roundtrip period, but these oscillations were damped. This suggests that the undamped oscillations can prevent the realization of stationary solitons with different pedestals. In any case there is the very large region D_i where the effects of period doubling are realized and this circumstance impedes to study the dependence of established stationary solitons with different pedestals on initial conditions. The question about any suppression of these effects in real experiment will not be discussed here. To attain this goal in numerical experiment, we will use the models with uniform spatial distribution of nonlinear losses in the next section.

In the case of Fig. 6 the soliton pedestal has not the fine oscillating structure. In the beginning of the transient process a symmetric ultrashort pulse is formed. However, the symmetric placement of the pulse on the pedestal is unstable. Depending on initial conditions, the main pulse is shifted to the leading front or to the trailing edge of the pedestal. The asymmetric soliton has two stable states: with left and right asymmetries. The corresponding temporal (spectral) distributions are transformed one into the other by changing the sign of the horizontal axis in Figs. 6(c) and 6(d). The solitons with different asymmetries move relative to each other, relative to unstable symmetric isolated solitons, and to stable symmetric soliton structures. Figure 7 shows the nonelastic collision of such two solitons with opposite asymmetries. After the collision the stationary symmetric structure with two bound solitons is realized.

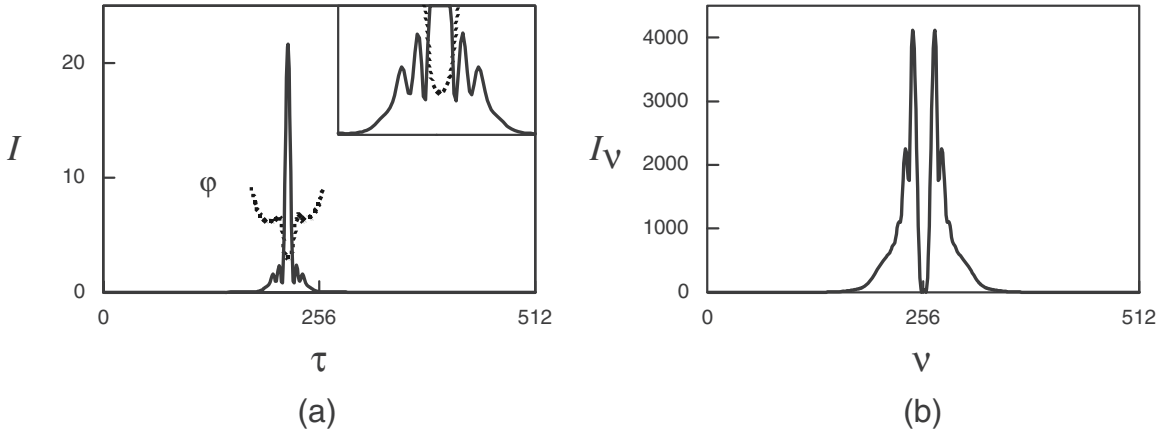

FIG. 3. Temporal (a) and spectral (b) distributions for the soliton in the fiber laser with anomalous dispersion with $D_i=1.0$. The other parameters are the same as in the case of Fig. 2. The change of phase φ along the soliton is shown by the dash curve in (a).

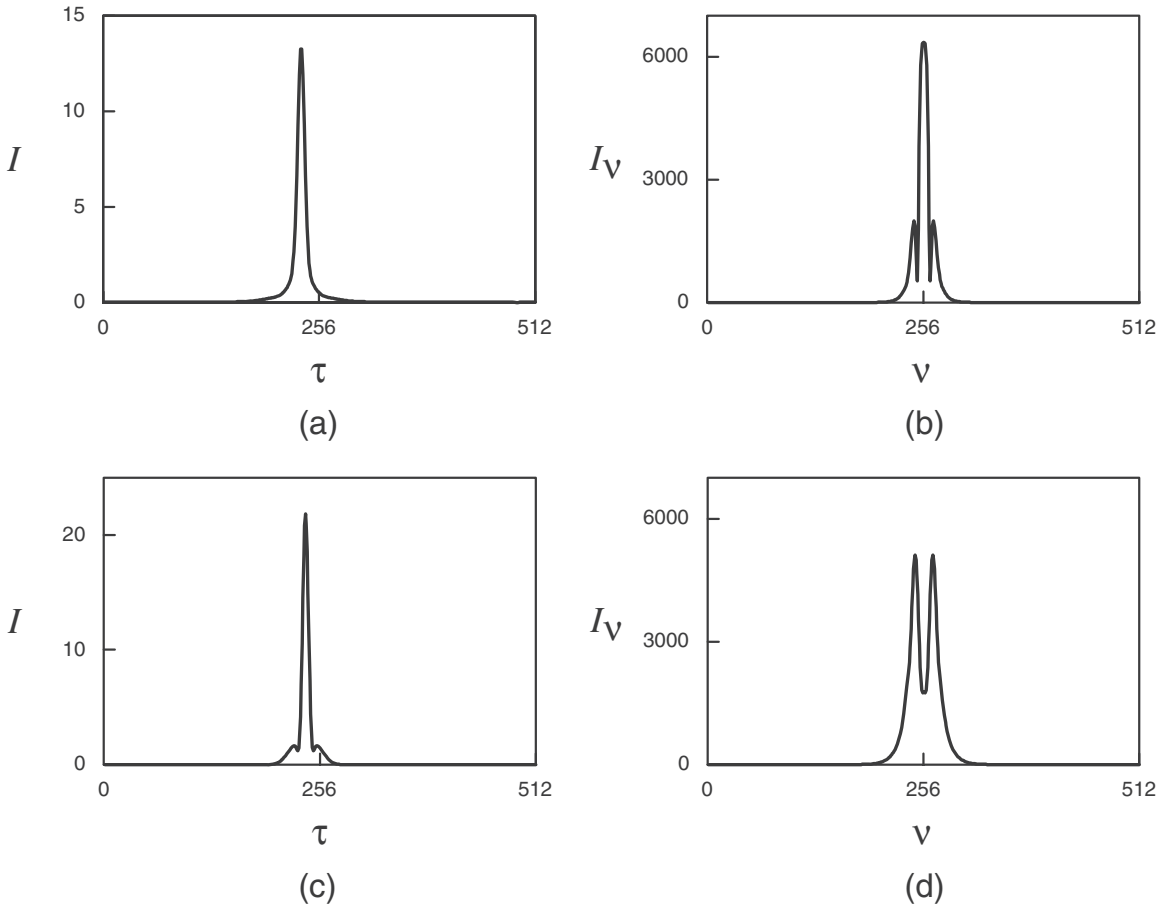

FIG. 4. Two types of solitons with different temporal (a), (c) and spectral (b), (d) distributions which are realized with the same laser parameters. $a=1.32$, $D_i=0.935$, $D_r=0.05$, $\alpha_3=0.11$. The other parameters are the same as in the case of Fig. 2.

III. MODELS WITH UNIFORM SPATIAL DISTRIBUTION OF NONLINEAR LOSSES

In the case of lumped nonlinear losses, the soliton, passing through the cavity, experiences the impact action of nonlinear losses with a period equal to the roundtrip one. This periodic action is favorable for a realization of period-doubling regimes that masks the investigated phenomena. The existence of different soliton states with closed energies is also favorable for such regimes. To prevent the masking action of period-doubling regimes, we used the models with

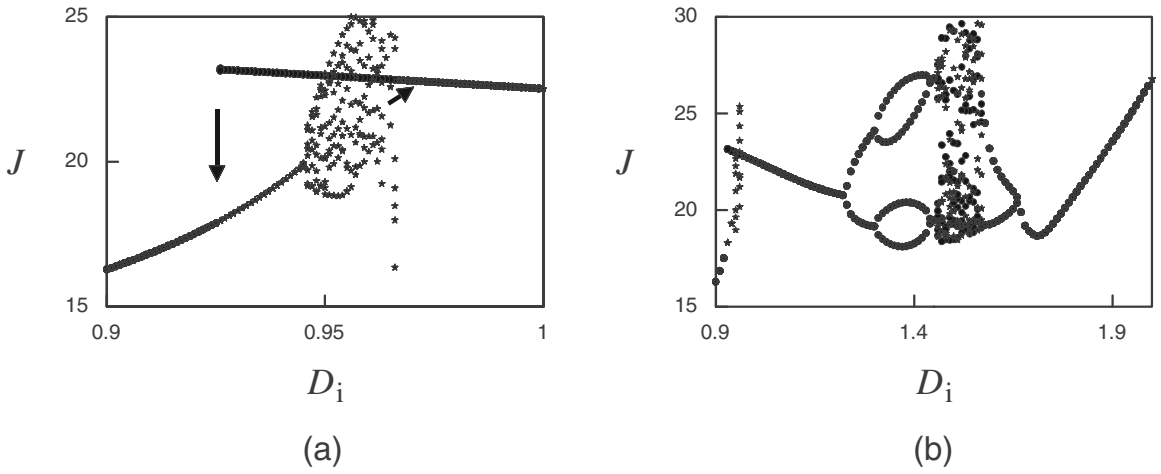

FIG. 5. Energy of the soliton J after its every passage through the laser cavity as a function of the dispersion D_i presented on enlarged (a) and reduced (b) scales. The laser parameters are presented in Fig. 4. The chaotic fragment of the dependence in (a) is connected with the down part of the hysteresis loop.

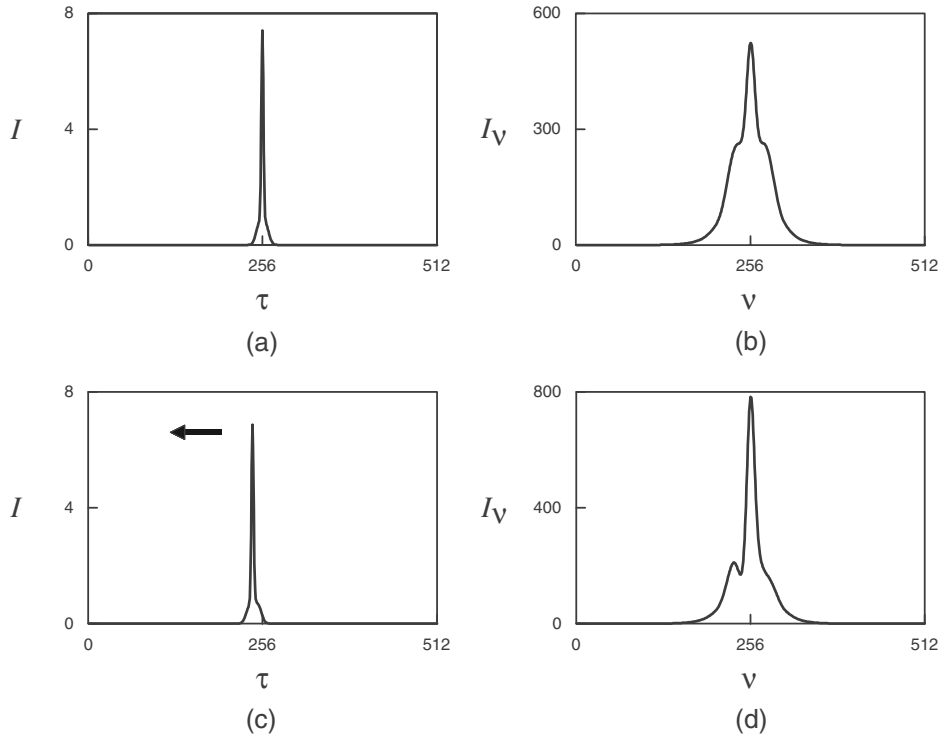

FIG. 6. Symmetric temporal (a) and spectral (b) distributions for the dissipative soliton establishing in the beginning of the generation $\zeta=100$. Because of the instability of symmetric soliton, after transient process the ultrashort pulse with asymmetric temporal (c) and spectral (d) distributions is realized. $a=1.2$, $q=2$, $D_i=0.13$, $D_r=0.001$, $\alpha=0$, $\alpha_1=-1.64$, $\alpha_3=0.2$.

uniform spatial distribution of nonlinear losses.

From Eq. (2) we obtain

$$I_{n+1}(\tau) = \eta^2[\cos^2(\alpha_1 - \alpha_3) - \cos 2\alpha_1 \cos 2\alpha_3 \sin^2(pI_n + \alpha_0)]I_n(\tau). \tag{4}$$

This nonlinear transmission of the radiation through the polarizing isolator could be modeled by the following distributed nonlinear losses $[-\sigma_0+\sigma \sin^2(pI+\alpha_0)]$ where σ_0, σ, p, α_0 are independent parameters determining these losses, $\sigma < \sigma_0$. Correspondingly, the master equation has the following form:

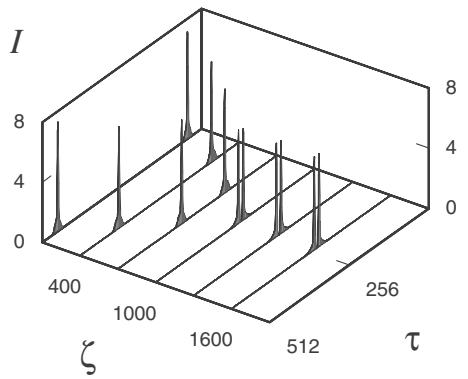

FIG. 7. Nonelastic collision of asymmetric solitons. $a=1.26$, the other parameters are the same as in the case of Fig. 6.

$$\frac{\partial E}{\partial \zeta} = (D_r + iD_i)\frac{\partial^2 E}{\partial \tau^2} + [G + iq|E|^2 - \sigma_0 + \sigma \sin^2(pI + \alpha_0)]E. \tag{5}$$

This is the model equation describing adequately at qualitative level many properties of passive mode-locked fiber lasers.

Figure 8 demonstrates the multistability of the single soliton regime. With the same laser parameters we observed the five different isolated solitons having different pedestal structures and spectral distributions. Each of these solitons is stationary. After transient process its spectral and temporal distributions do not vary with increasing number of passes of radiation through the laser cavity. The realization of one or the other type of a stationary soliton depends on initial conditions.

Figure 9 demonstrates the regime of the asymmetric isolated soliton obtained in the frame of the distributed model described by cubic-quintic CGLE,

$$\frac{\partial E}{\partial \zeta} = (D_r + iD_i)\frac{\partial^2 E}{\partial \tau^2} + [G - 1 + (p + iq)|E|^2 + (\tilde{p} + i\tilde{q})|E|^4]E. \tag{6}$$

The formation of the top part of the soliton shown in Fig. 9 is mainly related with the frequency dispersion D_i and the quintic nonlinearity $\tilde{q}$ of refractive index of intracavity medium. This asymmetric soliton in its properties is similar to the asymmetric one shown in Fig. 6, nevertheless there are significant differences. This circumstance is discussed below.

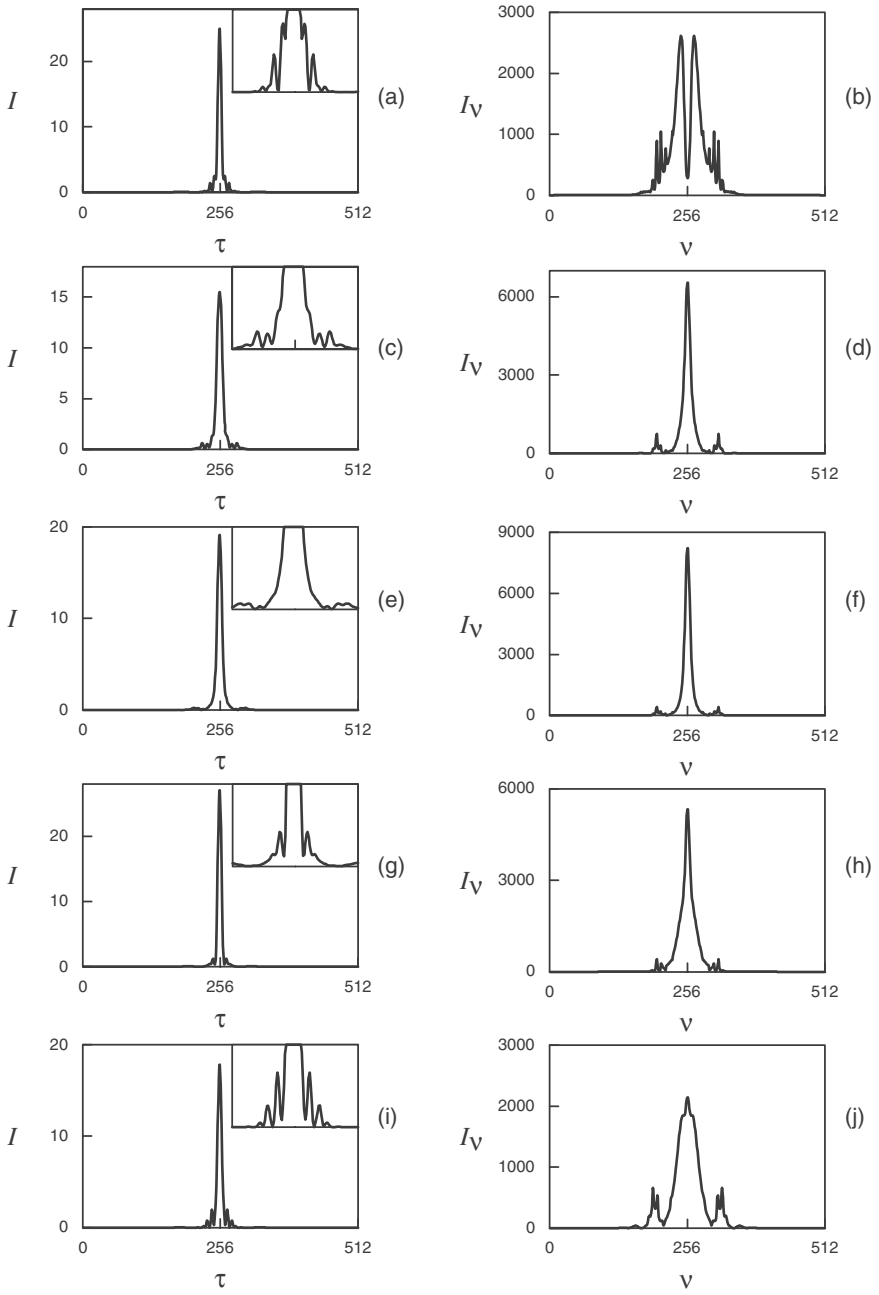

FIG. 8. Temporal $I=I(\tau)$ and spectral $I_\nu=I_\nu(\nu)$ distributions for the five different solitons realizing with the same laser parameters in a single pulse operation. Realization of one or other soliton depends on initial conditions. $a=1$, $q=1$, $D_i=1$, $D_r=0.05$, $\sigma_0=1$, $\sigma=0.9$, $p=0.1$, $\alpha_0=-0.2$.

IV. DISCUSSION

In the frame of the model described by the cubic CGLE [Eq. (6) with $\tilde{p}=0$, $\tilde{q}=0$], the steady-state soliton amplitude is determined by the expression (see, for example, [4])

$$E(\tau) = \frac{E_0}{\cosh^{1+i\alpha}(\beta\tau)}, \tag{7}$$

where E_0, β, α are the constants determining the peak amplitude, the inverse duration, and the chirp of the ultrashort pulse, accordingly. The phase change φ along the pulse is

$$\varphi(\tau) = -\alpha \ln\cosh(\beta\tau). \tag{8}$$

Correspondingly, the change of local frequency $\delta\omega$ (detuning of the local frequency from the center of the spectral amplification band) along the soliton is determined by the expression

$$\delta\omega(\tau) = \dot{\varphi}(\tau) = -\alpha\beta \tanh(\beta\tau). \tag{9}$$

The amplitude maximum places in the point $\tau=0$. Here the phase is stationary $\dot{\varphi}=0$, the detuning from the center of the frequency amplification band is equal to zero $\delta\omega=0$, and the amplification is maximum. With increasing $|\tau|$, the detuning

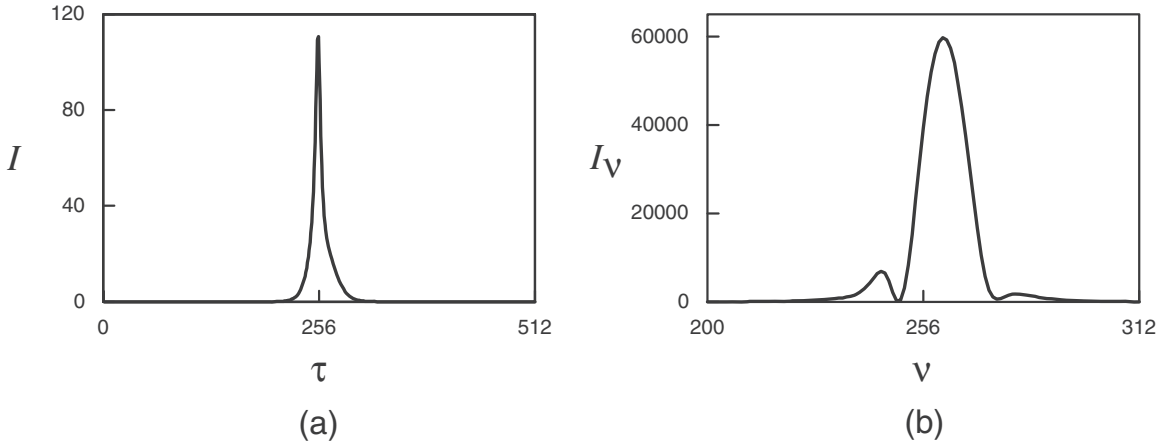

FIG. 9. Temporal and spectral distributions for the soliton obtained in the distributed model described by cubic-quintic CGLE. $a=1.5$, $D_i=1$, $D_r=0.2$, $p=10^{-2}$, $q=-10^{-2}$, $\tilde{p}=-10^{-4}$, $\tilde{q}=1.1\times10^{-4}$.

increases and the amplification falls. In the case of anomalous dispersion $D_i>0$, the phase modulations due to the focusing nonlinearity $q>0$ and the frequency dispersion of refractive index compensate for each other if $D_i/D_r=q/p$ [14]. In this case $\alpha=0$, the phase compensation is realized along total soliton. Such global phase compensation is possible thanks to chosen nonlinear-dispersion parameters of the laser systems (using of the model described by the cubic CGLE). If the nonlinear losses have any more complicated dependence on an intensity than the linear one the phase compensation is possible only in two symmetric points on wings of a soliton. In these points the phase is stationary ($\dot{\varphi}=0$). It means that detuning of carrier frequency from the center of the gain band for these points is equal to zero and the amplification is so efficient as in the soliton center, which is the point of the stationary phase. It is precisely the situation that is realized in our numerical experiment (see the phase dependence in Figs. 2 and 3). Such effective amplification at the soliton wings is one of main reasons of powerful soliton pedestals obtained in our numerical experiment.

Notice the limitation of the peak soliton intensity due to intracavity phase plates is also favorable for the realization of powerful pedestals with increasing pumping a. In this case, because of the peak intensity limitation, the pump energy is transformed into the additional pedestal energy. In addition, the wide spectral amplification band $D_r \ll D_i$ is favorable for the realization of intrasoliton structures.

As mentioned above, the top part of the soliton and its pedestal are formed by different mechanisms. The former is mainly shaped by the combined action of the focusing nonlinearity and the anomalous dispersion of refractive index. The latter is formed also by the nonlinear losses. The different mechanisms of shaping determine the essentially different profiles of these fragments of the soliton. The main part of the soliton through the boundary continuity conditions dictates the phase φ and its change rate $\dot{\varphi}$ in the pedestal. Since the dictated chirp $\dot{\varphi}$, as a rule, does not correspond to the equilibrium one of the pedestal, then the oscillation in the pedestal chirp is realized. This chirp oscillation results in the intensity oscillation in the pedestal. By such way the oscillating pedestal structure is realized. When the oscillation period becomes of the order of the pedestal length, because of a competition, the soliton pedestal wings turns out with different amplitudes, and the soliton becomes asymmetric. The frequency chirp determines the elastic properties of the soliton. Thanks to weak frequency chirp of pedestals, free solitons transform easily into bound solitons (see Fig. 7). Because of the powerful pedestal wings the bound energy turns out large. That is, the boundary solitons are very stable structures.

Parameters of dissipative solitons are usually determined by parameters of a laser system. Here we have found that soliton parameters can essentially depends on initial conditions. With the same laser parameters the different isolated solitons can be realized (see Fig. 8). Such multistability is due to the nonlinear properties of the investigated system. Thus, one can say about inherent structure of such dissipative solitons. It should be pointed that the qualitative correspondence of Figs. 2 and 3 to Fig. 8 lends support to the validity of the use of Eq. (5) for the description of passive mode locking in fiber lasers.

It should be noted that the pedestals of the asymmetric solitons shown in Figs. 6(c) and 9(a) are considerably different. The former is obtained from Eqs. (1) and (2), the latter is obtained from the cubic-quintic CGLE (6). This means that the use of the cubic-quintic CGLE must be done with some caution. The expansion of the nonlinear losses in a Taylor series assumes that a next term of the expansion is small in comparison with a previous one. In the case of the realization of asymmetric pedestals in the frame of Eq. (6), this condition turns out to be violated: with the used parameters of the cubic-quintic CGLE the cubic term is less than the quintic one. If we shall attempt to fulfill this condition then this means the following. The soliton is formed mainly by the cubic nonlinearity, and the quintic nonlinearity modifies only slightly the top of the soliton for which the quintic term in the CGLE has a maximum value. As this takes place, the soliton pedestal does not change practically because of fast decrease of the quintic term with decreasing intensity. Thus, the CGLE is not suitable for any analysis of the solitons with structural pedestals. Note, in the frame of the cubic-quintic CGLE the authors of the paper [15] obtained the symmetric

and asymmetric solitons only with the structural top. These solitons were named composite solitons and the moving ones, respectively. The cubic-quintic CGLE with the additional term proportional to the fourth derivative of field amplitude with respect to time (the complex quintic Swift-Hohenberg equation) can also demonstrate the many-valued dependence of the structure of established soliton on initial condition in the case of Eq. (5) [16]. However, this structure is only the structure of the soliton top, but not the pedestal, in agreement with the reasons presented above.

It should be noted that similar results on the soliton spectra with complex structure were reported in papers [17,18]. The structure of spectra were explained by period-doubling effects and by constructive interference between the soliton and the dispersive waves. These dispersive waves are emitted by the soliton when it circulates in the laser cavity and periodically experiences perturbations caused by the intracavity components. For solitons shown in Fig. 8 these mechanisms do not work, since the solitons are stationary and in the current model the intracavity medium has spatially uniform distribution, correspondingly the dispersive waves are not emitted. In our case the complicated structural spectra are connected with powerful structural pedestals of solitons. Such pedestals are due to specific intensity-dependent nonlinear losses arising in passive mode-locked fiber lasers exploiting nonlinear polarization rotation technique.

V. CONCLUSION

We found that in the passive mode-locked fiber lasers with anomalous dispersion the dissipative solitons with powerful structural pedestals can be realized. Such pedestal structures cause the complicated structural spectrum. The pedestal structure of steady-state single solitons can have a many-valued dependence on initial conditions: with the same laser parameters, the solitons with different pedestal structures are realized. In the case of pedestals without any fine structure, the solitons become asymmetric. The solitons with right and left asymmetric spectrum and temporal intensity distribution of the field move relative to each other and relative to symmetric bound and single solitons. The powerful pedestals of single solitons result in bound solitons with a large bound energy.

ACKNOWLEDGMENTS

This research was supported by Marie Curie International Fellowship within the 6th European Community Framework Programme (Contract No. 039942-PMLFL).

[1] M. Remoissenet, *Waves Called Solitons* (Springer-Verlag, Berlin, 1994).
[2] N. N. Akhmediev and A. Ankiewicz, *Solitons* (Chapman and Hall, London, 1997).
[3] I. S. Aranson and L. Kramer, Rev. Mod. Phys. **74**, 99 (2002).
[4] A. K. Komarov and K. P. Komarov, Phys. Rev. E **62**, R7607 (2000).
[5] N. N. Akhmediev, A. Ankiewicz, and J. M. Soto-Crespo, Phys. Rev. Lett. **79**, 4047 (1997).
[6] A. Komarov, H. Leblond, and F. Sanchez, Phys. Rev. A **71**, 053809 (2005).
[7] Ph. Grelu, F. Belhache, F. Gutty, and J. M. Soto-Crespo, Opt. Lett. **27**, 966 (2002).
[8] D. Y. Tang, B. Zhao, D. Y. Shen, C. Lu, W. S. Man, and H. Y. Tam, Phys. Rev. A **68**, 013816 (2003).
[9] N. N. Akhmediev, J. M. Soto-Crespo, M. Grapinet, and Ph. Grelu, Opt. Fiber Technol. **11**, 209 (2005).
[10] A. K. Komarov, Opt. Spectrosc. **102**, 637 (2007).
[11] A. Komarov, H. Leblond, and F. Sanchez, Phys. Rev. A **72**, 063811 (2005).
[12] D. M. McAvity, R. H. Enns, and S. S. Rangnekar, Phys. Rev. A **38**, 4647 (1988).
[13] N. Akhmediev, J. M. Soto-Crespo, and G. Town, Phys. Rev. E **63**, 056602 (2001).
[14] A. Komarov, H. Leblond, and F. Sanchez, Opt. Commun. **267**, 162 (2006).
[15] V. V. Afanasjev, N. Akhmediev, and J. M. Soto-Crespo, Phys. Rev. E **53**, 1931 (1996).
[16] J. M. Soto-Crespo and N. Akhmediev, Phys. Rev. E **66**, 066610 (2002).
[17] D. Y. Tang, L. M. Zhao, and F. Lin, Europhys. Lett. **71**, 56 (2005).
[18] D. Y. Tang, J. Wu, L. M. Zhao, and L. J. Qian, Opt. Commun. **275**, 213 (2007).